Materials Advances

ROYAL SOCIETY OF CHEMISTRY

PAPER

View Article Online
View Journal | View Issue

Cite this: *Mater. Adv.*, 2025, 6, 9516

Enzyme-containing double layer polymersomes coated by erythrocytes as a biomimetic nanoscavengers for *in vivo* protection from toxicants†

Tatiana Pashirova, *[ab] Dmitry Tatarinov, [b] Zukhra Shaihutdinova,[ab] Albina Malanyeva,[a] Olga Vasileva,[a] Alexey Rogov,[a] Vladimir Evtjugin,[a] Andrey Nemtarev,[b] Aida Gabdoulkhakova,[a] Eric Chabrière,[cd] Pauline Jacquet,[d] David Daudé[d] and Patrick Masson*[a]

A new strategy for effective antidotes against organophosphorus compounds (OPs) is enzyme-loaded nanoscavenger technology. Cell membrane-coated nanoforms of bioscavengers reduce adverse effects and ensure stability, immunotolerance, and prolonged protective action. For the first time, synthesis of double layers polymersomes coated by red blood cells (erythrocytes) ghosts, based on amphiphilic di- and triblock polyethylene glycol–polysulfide copolymers (PEG-*b*-PPS) was carried out to make enzyme microreactors. The enzyme was an evolved multiple mutant of the archaea *Saccharolobus solfataricus* phosphotriesterase (PTE). Two approaches were used for making this formulation: lipid fusion and hypotonic swelling. Respectively two types of PTE-loaded nanoscavengers (i) hybrid camouflaging RBC–PTE–loaded polymersomes and (ii) PTE–polymersomes captured by erythrocytes ghosts (PTE–RBC–microreactors) were prepared with high encapsulation efficiency, loading capacity and enzyme activity. CD-1 mice were challenged with paraoxon as a model OP. Pre-treatment of animals with *i.v.* injected PTE–RBC–microreactors led to LD_{50} shifts up to 15.5 times compared to control mice. In post-exposure treatments, LD_{50} shifts were up to 9.8 times. Pharmacokinetics of PTE–RBC–microreactors showed half times of 20 min and 1 hour for distribution and elimination phases, respectively. These first results with erythrocyte ghost microreactors are promising and open a new way to personalized medical countermeasures for detoxification of OPs and other toxicants.

Received 12th August 2025,
Accepted 15th October 2025

DOI: 10.1039/d5ma00894h

rsc.li/materials-advances

Introduction

The emergency treatment of poisoning by xenobiotics such as methanol, ethylene glycol, organophosphorus compounds is still imperfect,[1–3] because metabolic products formed during poisoning can be more dangerous than the parent toxicant itself or because of trapping toxic molecules in fat. Usually, antidotal therapy and accelerated elimination by dialysis are applicable. Antidotes used for organophosphorus poisoning, oximes, are not fully effective because they do not penetrate the central nervous system or do not reactivate certain cholinesterase–OP adducts.[4–6] Even oxime delivery systems are unable to reach the desired effect.[7–10] Today, the best detoxifying effect against OPs is provided by bioscavengers (OP-reacting enzymes such as butyrylcholinesterase and phosphotriesterases).[11–13] The advantage of bioscavengers is their lightning-fast binding to the toxicants, providing their rapid neutralization. Thus, toxicant molecules do not reach biological targets and will not harm the living organism. The disadvantages of bioscavengers are their high cost and the immune response induced by administration of heterologous enzymes. There are ways to reduce these drawbacks.[14,15] It should be mentioned that administration of homologous enzymes, does not induce immune response after the second injection.[16]

A new approach is to create nanoforms of bioscavengers.[17–20] Encapsulation of bioscavengers in nanoparticles ensure their stability, immunotolerance, prolongation and protective action

[a] *Institute of Fundamental Medicine and Biology, Kazan Federal University, 418 Kremlyovskaya St., 420008 Kazan, Russian Federation. E-mail: pashirova_tatyana@mail.ru, pym.masson@free.fr, masson.pym@gmail.com*
[b] *Arbuzov Institute of Organic and Physical Chemistry, FRC Kazan Scientific Center of RAS, Arbuzov Str. 8, 420088 Kazan, Russian Federation*
[c] *Aix Marseille Univ, IRD, APHM, MEPHI, IHU-Méditerranée Infection, 19-21 Boulevard Jean Moulin, 13005 Marseille, France*
[d] *Gene&GreenTK, 19–21 Boulevard Jean Moulin, 13005 Marseille, France*

† In memory of Dmitry Tatarinov. He passed away on March 13th, 2025 before the completion of this work.

in the body.[21–23] Various carriers such as liposomes, MOFs, polymeric nanoparticles, were applied for encapsulating enzymes like butyrylcholinesterase (BChE).[24] The high efficiency of nanoantidotes is achieved when the toxicant present in the bloodstream diffuses through the membrane of these nanoreactors to the sealed enzyme compartment, where the enzymatic detoxification reaction occurs.[23] Lightning-fast diffusion of the toxicant through the membrane is ensured by its reverse concentration and high concentration of the enzyme.[25] Enzyme nanocontainers must be completely sealed to prevent leaks. This implies a multilayer structure of nanoparticles. That is, the retention of therapeutic proteins inside nanoparticles for a long time can be ensured by multilayer membrane, for example, multivesicular liposomes (DepoFoam),[26–28] multiple emulsions using microfluidic devices,[29–32] polyelectrolyte layer-by-layer self-assemblies.[33–36] However, applications are limited by the difficulty of obtaining such structures and lack of mechanistic explanations for their action. Immobilization of enzymes on cartridges for extracorporeal dialysis can be an alternative to injectable bioscavengers.[37] However, long-term stability issue of such fragile reusable devices has limited its applicability.

A new approach with numerous advantages is the creation of biomimetic membrane materials.[38–41] Cell membrane-coated and biomimetic nanoparticles have longer circulation time, better pharmacokinetic profile and slower elimination from the body.[42–44] Various types of particles such as liposomes, poly(lactic-*co*-glycolic) acid (PLGA) nanoparticles, metal–organic framework (MOF), poly(ε-caprolactone)–poly(-ethylene glycol) have been used as cores for biomimetic shells.[45,46] The biomimetic approach has been applied for protection against OPs, for example, using BChE as a bioscavenger: more than 2×10^6 BChE tetrameric molecules were associated with red blood cells in a formulation.[47] Oil cores coated by red blood cell membrane,[48] MOF nanoparticles with double liposomal and erythrocyte membranes[49,50] and PLGA-nanoparticles[51] were used for *in vivo* protection against OPs.

In this work, for the first time, synthesis of double layers polymersomes coated by erythrocytes ghosts based on amphiphilic block copolymers PEG-*b*-PPS was carried out. Two approaches for coating of PEG-*b*-PPS polymersomes by erythrocyte ghosts (lipid fusion and hypotonic swelling (using hypertonic solution and co-incubation mixing) were used and compared (Fig. 1). Encapsulation of bioscavenger into polymersomes coated by erythrocytes ghosts with high loading capacity was implemented for preparation of nanoscavengers as new effective antidotes. Toxicological and pharmacokinetic investigations of double layer polymersome nanoscavengers were successfully performed in a mouse model of paraoxon poisoning.

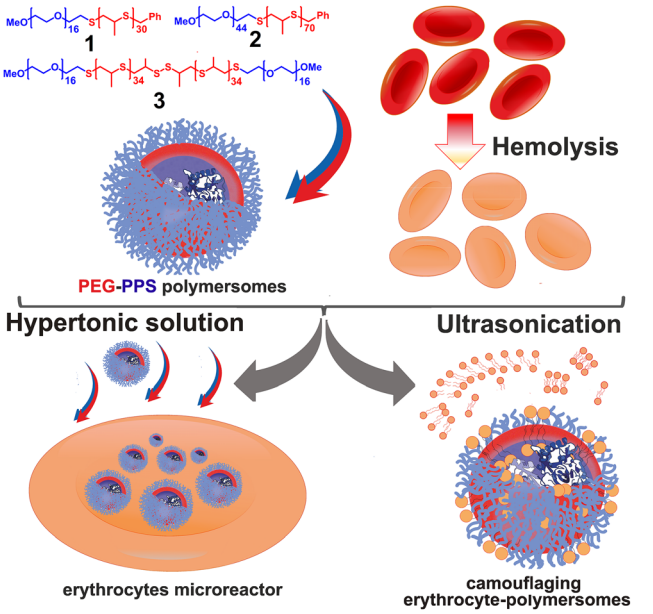

Fig. 1 Structures of di- and triblock copolymers PEG-*b*-PPS **1**, **2** and **3** and preparation of PTE containing double layer polymersomes coated by erythrocytes.

Experimental

Materials

The enzyme was a multiple mutant of the hyperthermophilic archaea *Saccharolobus solfataricus* phosphotriesterase (PTE)-like lactonase (PLL) that was functionally expressed in *E. coli* BL21(DE3). The enzyme is a dimer of 70 kDa (SsoPox-IIIC1). The method and all details of preparation and purification were previously described.[23,52,53] Specific chemicals were: propylene sulfide (stabilized with butyl mercaptan) (PS, Tokyo Chemical Industry Co., Ltd, Tokyo, Japan), poly(ethylene glycol)methyl ether with average M_n = 750 ($mPEG_{750}$, Sigma-Aldrich, USA), mPEG with average M_n = 2000 ($mPEG_{2000}$, Sigma-Aldrich, USA), potassium thioacetate (98%, Sigma-Aldrich, Switzerland), paraoxon-ethyl (POX, purity ≥90%, Sigma-Aldrich, product of Canada). All other chemicals were of analytical grade.

Synthesis of amphiphilic di- and triblock copolymers (PEG-*b*-PPS)

The synthesis of amphiphilic di- and triblock copolymers PEG-*b*-PPS **1**, **2** and **3** (Fig. 1) presented in Scheme S1 (SI) was described in previous works.[23,54,55] There were several stages in synthesis of thioacetate, namely thiolation of poly(ethylene glycol)methyl ether tosylate, to obtain thioacetate. Then, one pot method for preparation of **1–3** was applied. A detailed description of synthesis, structure conformation established by ^{1}H NMR and ^{13}C, and calculation of the hydrophilic fraction of PEG (f_{PEG}) using the ^{1}H NMR were presented earlier.[23,54] The optimal f_{PEG} of **1**, **2** and **3** PEG-*b*-PPS are 0.24, 0.27 and 0.23, respectively. These values are suitable for formation of polymersomes, and in agreement with literature data.[56–58]

Preparation of PTE-loaded polymersomes

PEG-*b*-PPS **1** was dissolved in 1 mL ethanol : chloroform (1 : 1). This solution was kept during 4 h at 33 °C for preparing the thin film and then overnight for residual solvent evaporation. PTE enzyme (12.5 and 25 μM) solution in Tris buffer (10 mM, pH 7.4) or in 0.9% NaCl was added to rehydrate the thin-film of

PEG-*b*-PPS at 37 °C. The solution was stirred, using a magnetic stirrer plate (Ika, Germany) at 600 rpm for 3 h at 37 °C, and then, kept overnight at room temperature.

Preparation of PTE-loaded double layer polymersomes coated by erythrocytes

There were two stages of preparation, first preparation of erythrocyte ghosts, and then, coating of PEG–PPS–polymersomes, using two approaches: hypotonic shock method and fusing erythrocyte ghosts with PTE-loaded polymersomes. All nanosystems coated with erythrocyte cell membranes were used on the day of preparation for all studies.

Preparation of erythrocyte ghosts. Haemoglobin-free erythrocyte ghosts were prepared according to a slightly modified method.[59] Heparinized blood (1.5 mL) from male mice-CD-1 was centrifuged (2500 rpm, 15 min) at 4 °C, and the supernatant plasma removed. Erythrocytes were washed three times with two volumes of phosphate buffer (0.1 M, pH 7.4) at 4 °C. Then, packed erythrocytes were diluted in about 150 volumes of hypotonic phosphate buffer (6.7 mM, pH 7.4) on ice to facilitate hemolysis, followed by centrifugation at 14 000 rpm for 30 min at 4 °C, using a Rotanta 460 centrifuge (Hettich Zentrifugen, Germany). The supernatant was subsequently removed. Three washing cycles were used for preparation of erythrocyte ghosts.

Fusing erythrocyte ghosts with PTE-loaded polymersomes. Prepared ghost aliquots in buffer solution (0.9% NaCl) were homogenized on ice with a Sonopuls HD 3010 ultrasonic homogenizer (Bandelin Electronic, Berlin, Germany) three times for 5 s at 30 s intervals with minimum energy. PTE (12.5 μM) in erythrocyte ghost solution (0.9% NaCl) from ~1.5 mL of whole blood was added to rehydrate the thin-film of PEG-*b*-PPS **1** at 37 °C and stirred, using a magnetic stirrer plate (Ika, Germany) at 600 rpm for 3 h at 37 °C, and then maintained overnight at room temperature.

Hypotonic swelling, using hypertonic buffer solution. Washed erythrocyte ghosts were resuspended and mixed with 2 mL of prepared PTE-loaded polymersomes solution (C_{PTE} = 12.5 μM) in Tris buffer (10 mM, pH 7.4) and kept for 15 minutes on ice. Then, hypertonic buffer solution (1.8% NaCl) in a ratio of 1 : 1 was added. The volume was adjusted to 2 mL using Amicon® Ultra-4 3 K centrifugal filters (Millipore Merck KGaA, Darmstadt, Germany) at 3000 rpm and 4 °C for 15 min, using a Rotanta centrifuge (Hettich Zentrifugen, Germany).

Hypotonic swelling, using co-incubation mixing. Purified erythrocyte ghosts were resuspended and mixed with 2 mL prepared PTE-loaded polymersomes solution (C_{PTE} = 12.5 μM) in isotonic 0.9% NaCl solution and kept for 30 min on ice.

Characterization of PTE-loaded double layer polymersomes coated by erythrocytes

Size, surface charge and morphology. A Malvern Instrument Zetasizer Nano (Worcestershire, UK) and Brookhaven 90Plus Nanoparticle Size Analyzer (Holtsville, New York, USA) were used to measure size, zeta potential and polydispersity index of nanoparticles. Dynamic light scattering (DLS) method allows to determine, the size (hydrodynamic diameter, nm), according to the Einstein–Stokes relationship $D = k_BT/3\pi\eta x$, in which D is the diffusion coefficient and x is the average hydrodynamic diameter of nanoparticles. Transmission electron microscopy (TEM) was used to image the size and to reveal the morphology. TEM images were obtained, using a Hitachi HT7700 (Exalens microscope, Japan). Images were acquired at an accelerating voltage of 100 keV. Samples ($C_{PEG-PPS}$ = 0.05 μg mL^{-1}) were added to a 300-mesh copper grid with continuous carbonformvar support films. High-resolution scanning electron microscope (SEM) Merlin (Carl Zeiss, Oberkochen, Germany) at an accelerating voltage of 5 kV was used to analyze the surface of erythrocyte ghost in the absence and presence of PEG–PPS polymersomes. The samples were fixed in 1% glutaraldehyde in phosphate buffer (0.1 M and pH 7.4 overnight), then in 2.5% glutaraldehyde for 2 hours, dehydrated in ethanol (30, 40, 50, 60, 70, 80, 90, and 96%). The specimens were mounted on aluminum stubs with double-sided carbon tape and sputter-coated with gold using the Q150T ES coater (Quorum Technologies, Lewes, UK).

Encapsulation efficiency (EE, %) and loading capacity (LC, %). EE and LC were calculated using eqn (1) and (2). These parameters were determined indirectly by filtration/centrifugation, measuring the free PTE by spectrophotometry. A volume 500 μL of sample was placed in a centrifugal filter device Amicon® Ultra-4 Centrifugal Filter Ultracel® 100 K (Millipore Merck KGaA, Darmstadt, Germany) for centrifugation (3000 rpm, 4 °C, 5 min), using a centrifuge (Eppendorf SE, Germany) to separate polymersomes and nonencapsulated PTE (free PTE). The concentration of free PTE in Tris buffer was quantified by absorbance using PerkinElmer Lambda 35 (PerkinElmer Instruments, USA) at 265 nm (ε = 93 333 M^{-1} cm^{-1}) in 10 mM Tris buffer, pH 7.4. UV absorbance spectra and calibrate curve are presented in SI file.[54]

$$\text{EE}\ (\%) = \frac{\text{Total amount of PTE enzyme} - \text{Free PTE enzyme}}{\text{Total amount of PTE enzyme}} \times 100\% \quad (1)$$

$$\text{LC}\ (\%) = \frac{\text{Total amount of PTE enzyme} - \text{Free PTE enzyme}}{\text{Total amount of PEG} - \text{PSS copolymer}} \times 100\% \quad (2)$$

Purification of PTE-loaded polymersomes and double layer polymersomes coated by erythrocytes. The same procedures and conditions were used as for the encapsulation efficiency study. The solution of PTE-loaded polymersomes was centrifuged, using Amicon® Ultra-4 Centrifugal Filter Ultracel® 100 K (Millipore Merck KGaA, Darmstadt, Germany) at 3000 rpm and 4 °C for 5 min in a centrifuge (Eppendorf SE, Germany). Upper layer of solution without free PTE was used for *in vitro* and *in vivo* studies.

PTE release study. This experiment was performed by the dialysis bag diffusion method, using spectra/Por® dialysis membrane (Biotech CE Tubing, MWCO: 100 kDa). The spectrophotometry method (Lambda 35, PerkinElmer Instruments, USA)

was used to detect PTE released from dialysis bag containing 1 mL PTE-loaded double layer polymersomes coated by erythrocytes. PTE extinction coefficient ε = 93 333 M^{-1} cm^{-1} at 265 nm in 10 mM Tris buffer, pH 7.4.[54] All details were described earlier in ref. 55 and 60. The receiving phase was 10 mL of 10 mM Tris buffer, pH 7.4.

PTE catalytic activity measurement

For free and encapsulated PTE measurements of catalytic activity, steady-state kinetics were recorded by monitoring the release of *p*-nitrophenolate (*p*Np) at 400 nm for 180 s with POX as the substrate at 25 °C in 10 mM Tris buffer, containing EtOH (1.5 vol%), pH 7.4, and supplemented with 0.2 mM $CoCl_2$, using Lambda 35 spectrophotometer (PerkinElmer Instruments, USA). POX concentration ranged from 5 to 1250 μM. Measurements were performed in triplicates. PTE hydrolyzes POX according to the classical Michaelis–Menten mechanism of enzyme kinetics, involving two steps: binding of substrate followed by kinetic step. Catalytic parameters (v – rate constant (velocity), min^{-1}; K_m – Michaelis constant, μM; k_{cat} – catalytic constant or turnover number, $V_{max} = k_{cat}[E]$ maximum reaction rate, min^{-1}) for hyperbolic dependencies $v = f(S)$ were determined, using the Michaelis–Menten eqn (3):[61]

$$v = \frac{k_{cat}[E][S]}{K_m + [S]} \quad (3)$$

where $[E]$ is the concentration of PTE and $[S]$ is the concentration of substrate POX. Rate data fitted with OriginPro 8.5 (Originlab Co., Northampton, MA, USA).

In vivo study

Animals. Mice-CD-1 (males, 6–10 weeks, 20–25 g) were used for experiments. They were maintained under standard conditions (12 h light/dark cycle; 22 ± 3 °C and a 50 ± 20% relative humidity). The adaptation time before starting experiment was at least 10 days. During this period, daily inspection of external animal conditions was carried out. All experimental procedures with animals were performed in accordance with the ethical principles in animal research and were approved by the local ethics committee of the Kazan Federal University (protocol no 40).

POX LD_{50} shifts in pre- and post-exposure treatments of mice. Mice were stratified by weight and randomly assigned into groups of three or six animals. POX was extemporaneously diluted in isotonic saline solution (0.9% NaCl) containing EtOH (10 vol%). POX LD_{50} were determined by subcutaneous (*s.c.*) injections at POX doses ranging from 0.5 to 0.7 mg kg^{-1}. Injections of 0.2 mL POX solution per 20 g animal were performed *s.c.*, using an insulin syringe (1 mL). 0.9% NaCl containing EtOH (10 vol%) solution (*s.c.*) was administered to a control group. Then LD_{50} determinations were performed after pre-treatment (prophylactic) and post-exposure (therapeutic) treatment of animals by PTE-loaded polymersomes or PTE-loaded double layer polymersomes coated by erythrocytes. 100 μL (PTE dose 3.7 mg kg^{-1}, PEG–PPS dose 25 mg kg^{-1}) was injected in tail vein, using insulin syringe 5 min before POX challenge (pre-treatment) and 1 min after POX challenge (post-exposure treatment). The initial POX doses were selected as the doses expected to cause mortality in some animals. Further groups of animals were dosed at higher or lower fixed doses, depending on the mortality in challenged animal groups, until the study objective was achieved. For each dose, 3 animals were used to minimize the number of animals. If in a group of 3 animals an unequivocal response was obtained (all animals died or survived), then we proceeded to the next dose. All animals were observed individually for symptoms and mortality after dosing with a special attention for the first 4 hours, and twice a day for two weeks after challenge. Poisoned animals that did not survive, died in less than 24 h. Died animals were autopsied. LD_{50} were calculated by Probit analysis using IBM SPSS Statistics software.

Pharmacokinetics in mice. The recommended maximum volume for *i.v.* administration in mice is 0.1 mL. Proceeding from this recommended volume, free enzyme solutions and PTE-loaded double layer polymersomes coated by erythrocytes (enzyme dose of 3.7 mg kg^{-1}) were slowly administered into the tail vein of mice weighing 20 g. Enzyme-loaded nanoreactor solutions were injected into the tail vein of each group animals. For each predetermined time interval (10, 30 min and 1, 2, 3, 4, and 24 h after injection) in each group, blood samples were collected into test tubes. After sampling, blood was centrifuged for 15 min under 2500 rpm at 4 °C, and the serum supernatant and erythrocytes were collected and frozen at −20 °C. PTE activity with POX as the substrate was subsequently assayed in each sample.

Results and discussion

Bioengineered strategies based on the use of cells[62] like red blood cells (RBC or erythrocytes) as drug delivery systems[63] are attractive due to their ability to evade the immune system, and thus, to perform the task for a more prolonged action in the body without adverse effects.[64–66] Erythrocyte-based delivery systems are ideal carriers for bioscavengers[67–69] because of their space of pharmacological activity is the blood and their ability to serve as long-term drug carrier in the bloodstream. Today, biotechnological methods for erythrocyte-based systems are expanding and including:[44,70] (i) surface modified RBCs or surface coupling, (ii) RBCs as carriers, including hybrid camouflaging of nanoparticles by wrapping them with fragments of RBC membrane. In turn, methods of internal loading into erythrocytes are divided into co-incubation, lipid fusion technique, osmosis-based method, electroporation and other tools.[71] Different ways of preparation for such systems affect their efficiency in terms of circulation and distribution times.[46]

Preparation of erythrocyte-coated PTE-loaded polymersomes

For preparation of erythrocyte-based systems loading PTE–enzyme, we implemented two approaches, namely the lipid fusion and the hypotonic swelling (Fig. 1). Lipid fusion technique allows to obtain hybrid camouflaging erythrocyte

nanoparticles. For the second approach, two methods were used: hypotonic/hypertonic solution transfer method and co-incubation mixing method. These led to the creation of polymersome containing RBC-microreactors.

The sterility of materials and solutions was maintained at all stages. First stage was preparation haemoglobin free erythrocyte ghosts, and then, there was coating of PEG–PPS polymersomes by erythrocyte membrane. The required volume of blood to cover all polymersomes was calculated, using several parameters: surface area, membrane thickness, concentration of RBC in mouse blood,[72,73] size and number of PTE-loaded polymersomes (SI). In the beginning, PTE was loaded into the polymersomes based on PEG-*b*-PPS **1**, using a slightly modified thin film method.[55] The enzyme concentration inside nanoparticles was chosen as optimal, based on our previous work.[54] This ''local'' concentration inside nanoparticles ensured a substrate reverse concentration gradient for its fast degradation within seconds. The block copolymer concentration was optimized to ensure the release of the reaction product, *p*Np, from nanoparticles. PTE-loaded polymersomes were characterized by DLS (Table 1, Fig. S1) and TEM (Fig. 2A and Fig. S2, SI). The size of obtained PTE-loaded polymersomes was about 160 nm (*Z*-average, nm), higher than the size of empty polymersomes (130 nm). Zeta potential (ξ) was about −7 mV, and PDI about 0.17 (Fig. S1, SI). TEM revealed spherical morphology and visible core–shell structure of PTE-loaded polymersomes (Fig. 2A and Fig. S2, SI). EE was rather high about 94 ± 1% with high loading about 16 ± 1% (Fig. S3, SI). PTE-loaded polymersomes were stable: storage for two months in a refrigerator at +4 °C had almost no effect on their characteristics. Increasing the enzyme concentration from 12.5 to 25 μM and PEG–PPS concentration from 5 to 10 mg mL^{-1} led to an increase the polydispersity of the systems. Comparison of characteristics (Table 1) with previous properties of nanoformulations for the same enzyme and different PEG-*b*-PPS indicates that the molecular weight of the PEG chain greatly affects the size. The size decreased from 160 nm to 106 nm with increasing PEG chain length from 750 (PEG-*b*-PPS 1) to 2000 (PEG-*b*-PPS 2) (Table 1 and Fig. S4, SI). PEG–PPS polymersomes based on PEG-*b*-PPS 2 with smaller size also had lower encapsulation efficiency (82 ± 7%). There was a small difference between the size of nanoparticles based on di- (PEG-*b*-PPS 1) and triblock (PEG-*b*-PPS 3) copolymers with PEG 750 (Table 1 and Fig. S4, SI). This resulted to a decrease in zeta potential from −7 to −19 mV, indicating a better stability.

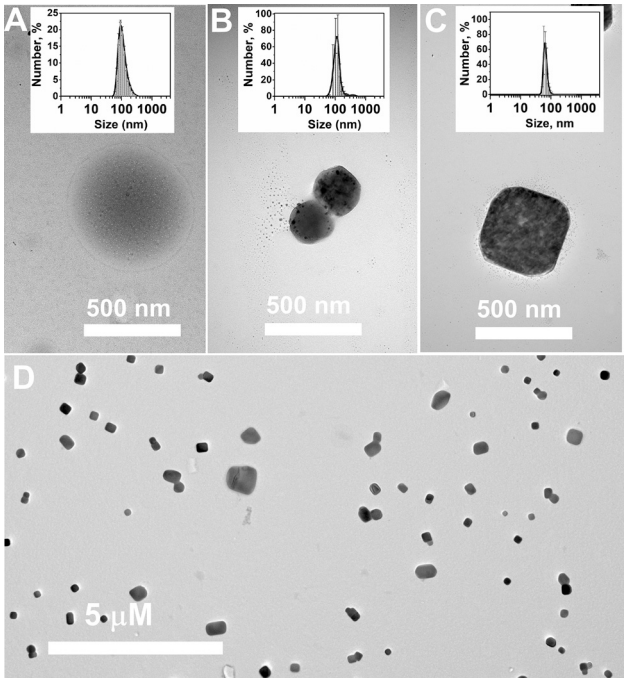

Fig. 2 TEM imaging and DLS data (distribution by number) of PTE–polymersomes in Tris buffer, pH = 7.4, (A), empty (B) and PTE-loaded (C, D) polymersomes coated by erythrocytes in 0.9% NaCl, C_1 = 0.05 μg mL^{-1}, 25 °C.

Creation of erythrocyte-based vehicles – polymersomes was carried out on PEG–PPS 1, *i.e.* nanosystem showing the highest EE, LC, the lowest polydispersity and a good stability. Hybrid camouflaging erythrocyte–polymersomes were prepared, using the lipid fusion technique. First, the isotonic suspension of hemoglobin free erythrocytes was subjected to ultrasonic homogenization to achieve a homogeneous matrix. Then, prepared polymeric thin of PEG–PPS 1 was hydrated by this homogeneous suspension of erythrocytes in different mass ratio (wt/wt) of 1 : 0.1; 1 : 0.2, 1 : 0.3, 1 : 0.5, 1 : 1. This method

Table 1 DLS data for PTE-loaded polymersomes based on PEG-*b*-PPS **1**, **2** and **3** in 10 mM Tris buffer and polymersomes coated by erythrocytes (**1**-RBC) in 0.9% NaCl–Tris buffer, pH = 7.4, 25 °C, size is hydrodynamic diameter, *Z*-average is the mean size, PDI is polydispersity index, ξ is zeta potential

			Size (nm)				
Nanoscavengers	$C_{PEG-PPS}$ (mg mL^{-1})	C_{PTE} (μM)	Int	Num	*Z*-aver (nm)	PDI	ξ (mV)
1[a]	5	—	142 ± 20	68 ± 13	130 ± 5	0.15 ± 0.01	−5.0 ± 2
1	5	12.5	164 ± 23	91 ± 20	161 ± 2	0.17 ± 0.01	−7.2 ± 1.4
1	5	25	173 ± 7	94 ± 8	154 ± 1	0.27 ± 0.01	−7.4 ± 0.9
1	10	25	178 ± 3	95 ± 5	161 ± 2	0.22 ± 0.01	−6.0 ± 0.6
1-RBC	5	—	125 ± 2; 500 ± 8	113 ± 13	—	0.23 ± 0.05	—
1-RBC	5	12.5	69 ± 3; 276 ± 20	62 ± 5	—	0.23 ± 0.05	—
1[b]	5	12.5	187 ± 16	94 ± 12	161 ± 2	0.19 ± 0.01	−7.0 ± 1.1
2[c]	5	12.5	106 ± 14	59 ± 12	106 ± 1	0.17 ± 0.01	−8.3 ± 0.3
3[d]	10	20	190 ± 20	79 ± 16	175 ± 1	0.18 ± 0.01	−19.0 ± 1

[a] From ref. 55. [b] Stability for 2 months at 4 °C. [c] From ref. 54. [d] From ref. 23.

allowed obtaining rather homogeneous nanoparticles without implementing extrusion through membranes.

The PDI of biomimetic erythrocyte-modified PEG–PPS nanoparticles ranged from 0.22 to 0.27 with increasing the content of erythrocytes (Table S1, SI). The particle size decreased and ξ became more electronegative with increasing erythrocytes content (Table S1, SI). The optimal ratio PEG–PPS 1: erythrocytes was 1 : 0.3, so it was used for further PTE loading. DLS data (Fig. S5–S7, SI) and TEM imaging (Fig. S8, SI) of hybrid camouflaging erythrocyte–polymersomes show large difference compared to uncounted PTE–polymersomes (Fig. 2). The successful modification of polymersome surface by erythrocyte lipids is visible. The slight decrease of the size is due to the isotonicity of buffer (Fig. S5, SI). Determination of EE showed close results 87 ± 7% and LC = 15% as for nonmodified PTE–polymersomes (Fig. S9, SI).

The second type of double layer polymersomes coated by erythrocytes – polymersome-containg RBC microreactors were prepared by incubation using two methods: in isotonic or in hypotonic/hypertonic buffer solutions. These methods are based on formation of transient openings in the RBC membrane *via* osmotic swelling in hypotonic solution. Co-incubation of purified erythrocyte membranes and PTE-loaded polymersomes in isotonic solution was not sufficient for complete coverage of erythrocyte membrane surface. Polymersomes were included only on the periphery of RBCs (Fig. S10, SI).

In this regard, this protocol was divided into two parts, namely, first, PTE-loaded polymersomes were mixed with purified RBC membranes in hypotonic solution. That is, polymersomes were loading through the membrane holes. Then, RBCs were sealed, using a hypertonic solution.

In this case, polymersomes were captured by RBCs (white specks) and looked like microreactors (Fig. 3A, Fig. S11, SI). This protocol of particle encapsulation in RBCs is based on the principle of hypotonic swelling where membrane pores can open, allowing nanoparticles to diffuse into the cell[74] before returning to isotonic conditions to seal the cell pores. PTE-loaded PEG–PPS polymeric nanoparticles captured by erythrocytes (microreactors) are systems with multi-compartment cellular architecture close to structures of molecular factories.[75] The encapsulation efficiency of PTE–microreactors is higher than for PTE–polymersomes and PTE-hybrid camouflaging erythrocyte–polymersomes and close to 99% (Fig. S12, SI). However, the dialysis method showed that PTE was released from these microreactors over time (Fig. 3B). Fig. S13 in SI shows spectra and enzyme release over time.

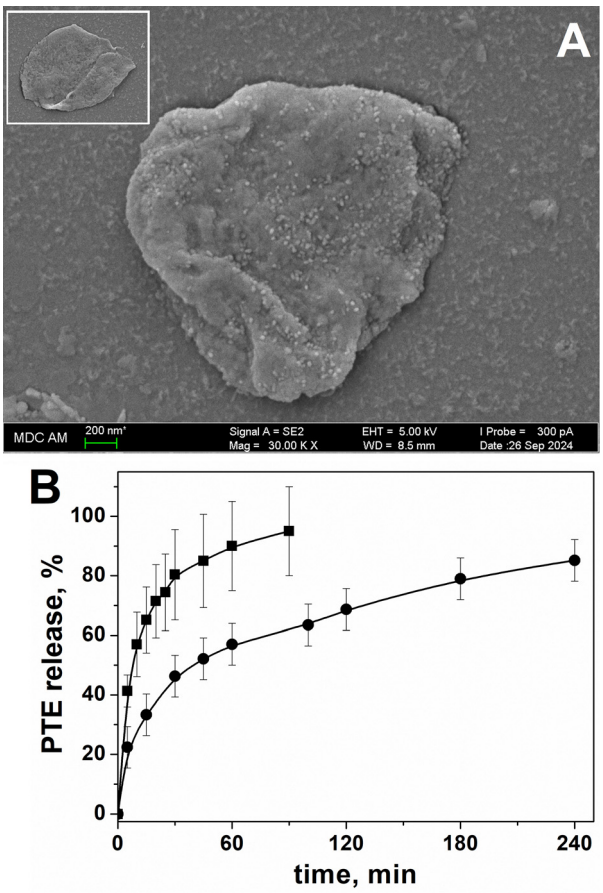

Fig. 3 Characteristics erythrocyte coated PTE–polymersome microreactors: SEM imaging (A) and release of PTE in 0.9% NaCl (B), insert in B: erythrocyte without PTE–polymersomes in hypotonic solution as a control.

Hydrolysis of substrate POX by encapsulated PTE under *in vitro* conditions

Before studying hydrolysis of POX catalyzed by PTE-loaded into nanoparticles, all types of nanoparticles were purified for removing external non-encapsulated enzyme. The enzyme concentration was determined by measuring the encapsulation efficiency of PTE. The reaction was monitored by the formation of reaction product *p*-Np. We previously shown that POX can easily penetrate into polymersomes due to high enzyme concentration "local concentration"[76] inside polymersomes (in the range of 0.17 ± 0.0189 and 0.93 ± 0.09 mM).[23] The number of enzyme molecules (N_E), taking into account the volume occupied by enzyme, is more than 300[77] with a turnover of 73.5 s^{-1} per active site[23] that is much more than the number of substrate molecules penetrating into the nanoparticles per second. This condition creates reverse gradient of substrate concentration, triggering rapid enzyme-mediated neutralization of substrate molecules. Our concept is opposite to that of ref. 78 where encapsulated single enzyme molecules in nanoparticles can be inhibited due to the high concentration of reaction products. In our system, the product *p*-Np formed during the reaction does not accumulate and leaves the inner core of polymersomes.[23] Thus, the aim of this work was to evaluate the influence of double membrane of PEG-*b*-PPS polymersomes on the kinetic parameters of the enzymatic reaction.

All kinetic curves are presented in Fig. S14 (SI). The hydrolysis of POX catalyzed by PTE and PTE-loaded into nanoparticles follows the classical Michaelis–Menten mechanism of enzyme. In all cases, the reaction rate as a function of POX concentration $v = f(S)$ is described by the hyperbolic michaelian saturation eqn (3) with r^2 = 0.98 (Fig. S15, SI) and Fig. 4. Thus,

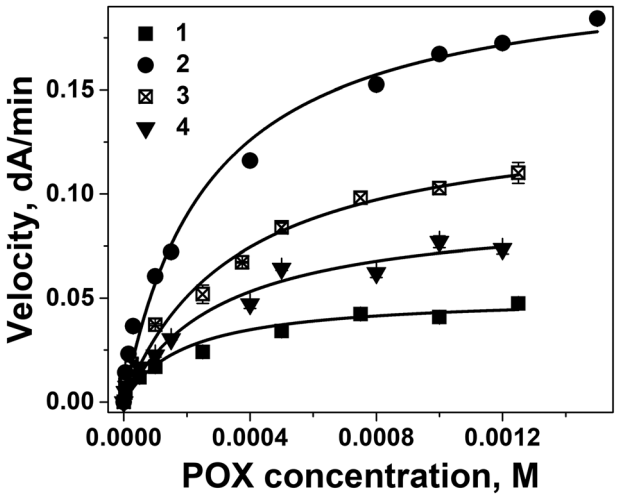

Fig. 4 Rate of POX hydrolysis catalyzed by PTE (1), PTE-loaded polymersomes (2), erythrocyte-modified PTE–polymersomes (3), erythrocytes coated PTE–polymersomes microreactor (4) on POX concentration in Tris/HCl (0.01 M) containing $CoCl_2$ (C = 0.0002 M) and ethanol 1.5% (vol), pH = 7.4, 25 °C.

the encapsulation of PTE into polymersomes (line 2), PTE-hybrid camouflaging erythrocyte–polymersomes (line 3) and erythrocyte-coated polymersome microreactors (line 4) does not change the reaction mechanism. The enzyme reaction parameters K_m and V_{max} were determined using the Michaelis–Menten eqn (3), then k_{cat} and the catalytic specificity (k_{cat}/K_m) were calculated. All catalytic parameters are presented in Table 2. Analysis of catalytic parameters shows a difference between free PTE (nonencapsulated) and encapsulated PTE:

(i) k_{cat} values of reference systems PTE–liposomes and PTE–solid lipid nanoparticles are lower than for PTE–polymersomes.

In addition, reference systems were not stable as a function of time at 4 °C.

(ii) k_{cat} values of encapsulated enzymes into PEG–PPS polymersomes are slightly increased (less than 3 times) compared to free enzyme values. This may be due to interactions of the enzyme with the internal membrane of nanoreactors, which has a beneficial effect on the enzyme dynamics or on the reaction taking place in a confined space. Authors[80] showed that k_{cat}/K_m was overestimated in the case of enzyme encapsulated in liposomes. Interestingly, the specific catalytic effect (k_{cat}/K_m) is decreasing in the same sequence as the size D (nm):

$$D_{\text{PTE–polymersome}} > D_{\text{PTE–camouflaging RBC–polymersomes}} > D_{\text{PTE–RBC microreactors}}$$

The effect of liposome size on internal reactions was analyzed.[81] The higher solute concentration in liposomes might account for high reactivity and the volume, which determines the concentration of included molecules,[82] is a key factor for the reaction occurring inside the compartment.[83]

(iii) The two methods used for erythrocyte coating of polymersomes had a moderate effect on all parameters. Thus, the double shell formed of polymersomes membrane and erythrocyte membrane coating does not affect the diffusion of POX to the active center of encapsulated enzymes. The substrate POX is an uncharged molecule of small molecular weight. In the literature free diffusion into liposomes is assumed only for small uncharged substrates[84,85] rarely without changing the catalytic parameters of enzymatic reactions.[86]

LD_{50} study

The approach based on coating nanoparticles with fragments of RBC membrane for detoxification of OPs has already been used applying the lipid fusion method.[49,50] Thus, our main interest is to develop this approach, using PTE-loaded polymersomes encapsulated into erythrocytes (erythrocyte–PTE–microreactors). As we know, such systems have been investigated here for the first time. For the *in vivo* experiment, the leader system – polymersomes-**1** with the highest EE, LC, low polydispersity, the best stability and good *in vitro* catalytic parameters was used. In a previous work, we showed that administration of PTE from *Saccharolobus solfataricus* caused a mild humoral response. In addition, challenged mice did not show observable physiological and behavioral effects after a second injection.[54] This makes our investigated nanosystems particularly safe and unable to trigger immune and adverse physiological responses. Looking ahead, our results showed that mild cellular, oxidative stress and cytokine responses took place, causing only mild transitory adverse effects (Gabdoulkhakova A. G. *et al.* article in preparation). To determine LD_{50} of POX, a single subcutaneous (*s.c.*) injection was used. The nanoparticle solution was administered intravenously. Seven groups of animals (three animals in each group) were used: two

Table 2 Catalytic parameters for PTE-catalyzed hydrolysis of POX in Tris/HCl (0.01 M) containing $CoCl_2$ (C = 0.0002 M) and ethanol 1.5% (vol), pH = 7.4, 25 °C

Systems	V_{max}, dA min^{-1}	k_{cat}, s^{-1}	K_m, μM	k_{cat}/K_m, ×10^5, M^{-1} s^{-1}
PTE	0.054 ± 0.004	29 ± 2	250 ± 54	1.16 ± 0.37
PTE–polymersomes	0.209 ± 0.01	65 ± 3	265 ± 44	2.45 ± 0.68
PTE–RBC–polymersomes	0.140 ± 0.01	74 ± 5	351 ± 67	2.1 ± 0.75
PTE–RBC–microreactors	0.093 ± 0.007	43 ± 3	303 ± 64	1.42 ± 0.47
PTE–liposomes[a]	0.061 ± 0.001	28 ± 0.5	70 ± 5	4.06 ± 0.94
PTE–solid lipid nanoparticles[a]	0.0027 ± 0.0001	45 ± 2.4	607 ± 75	0.74 ± 0.32

[a] Ref. 79.

Table 3 POX LD_{50} shifts at pre- and post-exposure treatments in mice

Systems	POX LD_{50} shift	
	Pre-treatment	Post-exposure
PTE–polymersomes-**1**	12.1	7.2
PTE–RBC–microreactors-**1**	11.7	8.9
PTE-loaded polymersomes-**2**[a]	15.6	5.3
PTE-loaded polymersomes-**3**[b]	16.6	9.8

[a] Dose of PTE = 3.7 mg kg^{-1}.[54] [b] Dose of PTE = 6.6 mg kg^{-1}.[23]

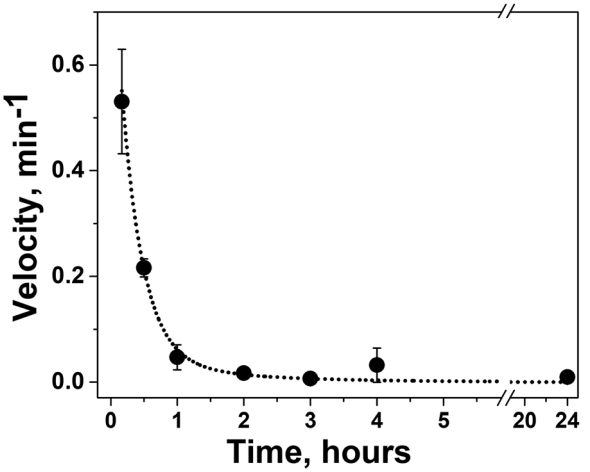

Fig. 5 PK of PTE in mouse plasma after intravenous injection of erythrocyte–PTE–microreactors. PTE dose 3.7 mg kg^{-1}, PEG–PPS dose 25 mg kg^{-1}. Each point represents the mean ± SD in four mice.

control groups (*i.v.*) polymersome solution without PTE in 0.9% NaCl and *s.c.* solution 0.9% NaCl containing ethanol (10 vol%). The third group received doses of POX from 0.25 to 0.7 mg kg^{-1}. The fourth group received PTE-loaded-polymersomes solution and 5 minutes later POX with doses ranging from 5 to 15 mg kg^{-1} (pre-treatment). The fifth group received POX at dose from 2.5 to 10 mg kg^{-1} and 1 min later PTE-loaded-polymersomes solution was injected (post-exposure treatment). The sixth and seventh groups were pre- and post-exposure treatment received erythrocyte–PTE–microreactors with POX dose ranging from 1.5 to 10 mg kg^{-1} and from 1.5 to 7 mg kg^{-1}, respectively.

Animals treated with empty polymersomes and solvent (10% EtOH) showed no clinical signs. Results about the acute toxicity study of POX are presented in Table S2 (SI). As a result of POX *s.c.* administration, depression of animal activity, dyspnoea, and convulsions were observed immediately after injections; death occurred within 20 min. Pathomorphological autopsy of animals revealed lung damage in some mice. LD_{50} of POX was 0.6 mg kg^{-1}. High *in vivo* protective efficacy against POX (*s.c.*) was established for both prophylactic and therapeutic administration PTE-loaded nanoparticles (Table 3). The highest LD_{50} shift was 15.6 for prophylactic administration of PTE-loaded polymersomes based on diblock PEG-*b*-PPS **2**. For therapeutic administration, the most effective is erythrocyte–PTE–microreactors-**1** with LD_{50} shift ~9. Therefore, PEG–PPS–polymersomes coating by biomimetic erythrocyte layer, showing improved detoxifying action are a promising approach for both pre-treatment (prophylaxis) and post exposure treatment of emergency acute OP poisoning.

Then, we studied the pharmacokinetics of erythrocyte–PTE–microreactors-**1** intravenously injected to mice for comparison with pharmacokinetics of PTE-loaded polymersomes-**2**. PTE activity with POX as the substrate was assayed in plasma (Fig. S16, SI). The pharmacokinetic curve is in Fig. 5. Time plots from the intravenous route of erythrocyte–PTE–microreactors administration were fitted (r^2 = 0.968, Fig. S17, SI) to the two-compartment pharmacokinetic model (eqn (4)):

$$[E]_t = Ae^{-\alpha t} + Be^{-\beta t} \quad (4)$$

where E_t is the PTE activity at time t, α and β are distribution and elimination rate constants, respectively. The calculated pharmacokinetic parameters are in Table 4, where $t_{1/2\alpha} = \ln 2/\alpha$, according to eqn (4) in which α is the distribution rate (h^{-1}) from blood and $t_{1/2\beta} = \ln 2/\beta$, according to eqn (4) in which β is the elimination rate (h^{-1}) from blood. As seen, the distribution phase for PTE–microreactors-**1**, PTE–polymersomes-**1** and nonencapsulated PTE is almost the same ~20 min.[54] On the other hand, there is a difference in the elimination phase.

The elimination phase for microreactors is more than 1 hour. Likely, the greatest effect in post-exposure treatment for PTE–microreactors-**1** (LD_{50} shift = 8.9) compared to PTE–polymersomes-**1** (LD_{50} shift = 5.3) could be explained by the longest elimination phase for PTE–erythrocyte microreactors-**1**. It may be stated that the longest elimination phase of PTE–erythrocytes microreactors is due to transfer of PTE–PEG–PPS polymersomes from RBCs to endothelium in the vasculature. This "RBC-hitchhiking" was shown for RBC–PLGA-nanoparticles.[87,88] In our previous work, the direct biodistribution of enzyme-encapsulated PEG–PPS 1 polymersomes in organs (IVIS imaging) provided evidence for elimination of nanoreactors by the liver but *via* different pathways unlike the free enzyme.[55] It needs to require further assessment in highly vascularized organs for PTE–microreactors in a future. Application of biomimetic microreactors and double coating of enzyme are more promising for post-exposure treatment of organophosphorus poisoning than for pre-treatment. The creation of formulations with a biomimetic membrane requires additional research and effort. Since particles can quickly detach from red blood cells,[89] which facilitates a rapid distribution phase for the enzyme. Change of deformability,

Table 4 Pharmacokinetic parameters

System	α (h^{-1})	$t_{1/2\alpha}$ (h)	β (h^{-1})	$t_{1/2\beta}$ (h)
PTE–microreactors-**1**	3.15 ± 0.91	0.22 ± 0.064	0.683 ± 0.067	1.015 ± 0.1

mechanical flexibility and physical sturdiness of RBCs can be caused by attached nanoparticles[90] and can accelerate RBC clearance. Also it is known that senescent red blood cells can be recognized and removed by the cellular immune system.[91]

Future work will focus on cellular immune reactions, optimization of the composition of erythrocyte–PTE–microreactors and to use different types of cell materials.

Conclusions

The creation of enzyme microreactors based on cell–membrane coated polymersomes is an extension of the concept of enzyme-loaded nanoscavengers. In the present work, we demonstrated that a highly toxic OP, POX, can be effectively detoxified *in vivo*, after injection to mice of double membrane enzyme reactors. This proof of concept shows that inclusion of numerous enzyme nanoscavengers in erythrocyte ghosts is a step forward the use of cocktails of multiple therapeutic enzymes for pleiotropic effects or for targeting numerous types of toxicants. The external envelope of the ''therapeutic bag'', erythrocyte membrane, links the multiple potential uses of this new technology to personalized medicine. However, the road to practical implementation of these enzyme microreactors at the bedside of patients is still long. As enzyme–RBC–polymersome microreactors is a novel biomimetic nanoplatform. Therefore, in future, several quality controls need to be explored: cell collection and isolation process, sterilization, optimization of the ratio of biological and synthetic components. All of these affect storage and long-term stability.[92,93] In particular, addition of cryoprotectants with the goal of minimizing membrane damage during storage in freezing conditions is planned. Other types of natural cell membranes or artificial membranes will certainly lead to practical formulations more stable than erythrocyte ghosts and easier to fabricate.

Author contributions

The manuscript was written through contributions from all authors. All authors have given approval to the final version of the manuscript. TP and ZS prepared and controlled the enzyme polymersomes, RBC ghosts and microreactors, DT and AN synthesized the block-copolymers, AM and OV performed animal studies, AG – investigated immunological reactions, PJ, EC and DD prepared enzyme, AR and VE performed macroscopy study, PM coordinated the work and wrote the manuscript with TP.

Conflicts of interest

The authors declare the following competing financial interest(s): E. C. and D. D. have filed the patent FR3068989. P. J., D. D., and E. C. report receiving personal fees from Gene&GreenTK during the study. E. C. and D. D. are shareholders in Gene&GreenTK. D. D. is CEO of Gene&GreenTK. E. C. and D. D. have filed the patent FR3068989. The other authors declare no conflicts of interest.

Data availability

The data supporting this article have been included as part of the supplementary information (SI). Supplementary information: Scheme S1 General scheme of synthesis of block-copolymers. 1. Calculation the amount of blood required to cover PTE-polymersomes. Fig. S1 Screen shot of PTE-loaded polymersomes size distribution. Fig. S2 TEM images of PTE-loaded polymersomes. Fig. S3 UV Absorbance spectra of PTE after ultracentrifugation of PTE-loaded polymersomes. Fig. S4. Size distribution of PTE-loaded polymersomes based on di- and triblock copolymers. Table S1 Dynamic light scattering data for erythrocyte membrane-camouflaged polymersomes Fig. S5 Size distribution of PTE-loaded polymersomes. Fig. S6 Size distribution for empty and PTE-loaded erythrocyte membrane-camouflaged polymersomes. Fig. S7 Screen shot for size distribution and correlation curves empty and PTE-loaded polymersomes. Fig. S8 TEM imaging of erythrocyte membrane-camouflaged PTE-polymersomes. Fig. S9 UV Absorbance spectra of PTE after ultracentrifugation of erythrocyte membrane-camouflaged PTE-polymersomes. Fig. S10 SEM imaging of erythrocyte coated PTE-polymersomes microreactor. Fig. S11 SEM imaging of erythrocyte coated PTE-polymersome microreactor. Fig. S12 UV Absorbance spectra of PTE after ultracentrifugation of erythrocyte coated PTE-polymersome microreactor. Fig. S13 UV Absorbance spectra of PTE release from erythrocyte coated PTE-polymersome microreactor. Fig. S14 Kinetic curves of POX hydrolysis by PTE. Fig. S15 Dependences of POX hydrolysis by PTE. Table S2 Prophylaxis and post-exposure treatment of paraoxon *s.c.* acute toxicity by *i.v.* administration of PTE-loaded nanoreactors in mice. Fig. S16 Kinetics of the POX hydrolysis by erythrocyte coated PTE-polymersome microreactors in mouse plasma. Fig. S17 Pharmacokinetics of PTE in mouse plasma after *i.v.* injection of erythrocyte coated PTE-polymersome microreactors. See DOI: **https://doi.org/10.1039/d5ma00894h**.

Acknowledgements

This work was supported by Grant from the Academy of Sciences of the Republic of Tatarstan, provided to young candidates of science (postdoctoral students) for the purpose of defending a doctoral dissertation, carrying out research work, and also performing work functions in scientific and educational organizations of the Republic of Tatarstan within the framework of the State Program of the Republic of Tatarstan ''Scientific and Technological Development of the Republic of Tatarstan''.

References

1 C. Humphries, M. Eddleston and J. Dear, *Medicine*, 2024, **52**, 56–61.

2 J. E. Perkins, K. E. Hovda, F. R. Chowdhury, J. B. Sørensen, M. Eddleston and A. Street, *Alcohol Alcohol.*, 2025, **60**(3), agaf018.
3 J. Alva, E. S. Devi, R. Chandrababu, J. Abraham and J. M. Balakrishnan, *Clin. Epidemiol. Global Health*, 2025, **32**, 101932.
4 Z. Kovarik, G. Moshitzky, N. Maček Hrvat and H. Soreq, *J. Neurochem.*, 2024, **168**, 355–369.
5 Z. Kohoutova, E. Prchalova, K. Knittelova, K. Musilek and D. Malinak, *Bioorg. Chem.*, 2024, **150**, 107526.
6 H. Thiermann, F. Worek and G. Horn, *Clin. Toxicol.*, 2025, 1–18.
7 T. N. Pashirova, I. V. Zueva, K. A. Petrov, V. M. Babaev, S. S. Lukashenko, I. K. Rizvanov, E. B. Souto, E. E. Nikolsky, L. Y. Zakharova, P. Masson and O. G. Sinyashin, *ACS Appl. Mater. Interfaces*, 2017, **9**, 16922–16932.
8 T. N. Pashirova, A. Braïki, I. V. Zueva, K. A. Petrov, V. M. Babaev, E. A. Burilova, D. A. Samarkina, I. K. Rizvanov, E. B. Souto, L. Jean, P.-Y. Renard, P. Masson, L. Y. Zakharova and O. G. Sinyashin, *J. Controlled Release*, 2018, **290**, 102–111.
9 D. N. Buzyurova, T. N. Pashirova, I. V. Zueva, E. A. Burilova, Z. M. Shaihutdinova, I. K. Rizvanov, V. M. Babaev, K. A. Petrov and E. B. Souto, *Toxicology*, 2020, **444**, 152578.
10 D. A. Kuznetsova, G. A. Gaynanova, E. A. Vasilieva, R. V. Pavlov, I. V. Zueva, V. M. Babaev, D. M. Kuznetsov, A. D. Voloshina, K. A. Petrov, L. Y. Zakharova and O. G. Sinyashin, *Pharmaceutics*, 2022, **14**, 1950.
11 L. Poirier, P. Jacquet, L. Plener, P. Masson, D. Daudé and E. Chabrière, *Environ. Sci. Pollut. Res.*, 2021, **28**, 25081–25106.
12 T. Pashirova, R. Salah-Tazdaït, D. Tazdaït and P. Masson, *Int. J. Mol. Sci.*, 2024, **25**, 7822.
13 Y. A. Mokrushina, A. V. Golovin, I. V. Smirnov, S. D. Chatziefthimiou, A. V. Stepanova, T. V. Bobik, A. O. Zalevsky, A. S. Zlobin, K. A. Konovalov, S. S. Terekhov, A. V. Stepanov, S. O. Pipiya, O. G. Shamborant, E. Round, A. A. Belogurov, G. Bourenkov, A. A. Makarov, M. Wilmanns, J. Xie, G. M. Blackburn, A. G. Gabibov and R. A. Lerner, *Proc. Natl. Acad. Sci. U. S. A.*, 2020, **117**, 22841–22848.
14 B. N. Novikov, J. K. Grimsley, R. J. Kern, J. R. Wild and M. E. Wales, *J. Controlled Release*, 2010, **146**, 318–325.
15 M. Trovaslet-Leroy, L. Musilova, F. Renault, X. Brazzolotto, J. Misik, L. Novotny, M.-T. Froment, E. Gillon, M. Loiodice, L. Verdier, P. Masson, D. Rochu, D. Jun and F. Nachon, *Toxicol. Lett.*, 2011, **206**, 14–23.
16 W. Sun, C. Luo, R. S. Naik, B. P. Doctor and A. Saxena, *Life Sci.*, 2009, **85**, 657–661.
17 Y. Liu, J. Li and Y. Lu, *Adv. Drug Delivery Rev.*, 2015, **90**, 24–39.
18 J. Yang, H. Li, H. Zou and J. Ding, *Chem. – Eur. J.*, 2023, **29**(42), e202301107.
19 B. Lu, L. Wei, G. Shi and J. Du, *Adv. Sci.*, 2024, **11**(15), 2308241.
20 T. N. Pashirova, Z. M. Shaihutdinova, V. F. Mironov and P. Masson, *Acta Nat.*, 2023, **15**, 4–12.
21 S. Zou, Q. Wang, J. Song, G. Liu, F. Zhang, J. Li, F. Wang, Y. Hu, Y. Lv, D. Zhou, Q. He, B. Wang and L. Zhang, *Giant*, 2024, **17**, 100213.
22 P. Zhang, E. J. Liu, C. Tsao, S. A. Kasten, M. V. Boeri, T. L. Dao, S. J. DeBus, C. L. Cadieux, C. A. Baker, T. C. Otto, D. M. Cerasoli, Y. Chen, P. Jain, F. Sun, W. Li, H.-C. Hung, Z. Yuan, J. Ma, A. N. Bigley, F. M. Raushel and S. Jiang, *Sci. Transl. Med.*, 2019, **11**, eaau7091.
23 T. Pashirova, Z. Shaihutdinova, M. Mansurova, R. Kazakova, D. Shambazova, A. Bogdanov, D. Tatarinov, D. Daudé, P. Jacquet, E. Chabrière and P. Masson, *ACS Appl. Mater. Interfaces*, 2022, **14**(17), 19241–19252.
24 T. N. Pashirova, A. Bogdanov and P. Masson, *Chem. – Biol. Interact.*, 2021, **346**, 109577.
25 Z. Shajhutdinova, T. Pashirova and P. Masson, *Biomedicines*, 2022, **10**, 784.
26 N. V. Katre, J. Asherman, H. Schaefer and M. Hora, *J. Pharm. Sci.*, 1998, **87**, 1341–1346.
27 Q. Ye, J. Asherman, M. Stevenson, E. Brownson and N. V. Katre, *J. Controlled Release*, 2000, **64**, 155–166.
28 J. Li, Z. Xia, M. Yu and A. Schwendeman, *Eur. J. Pharm. Biopharm.*, 2024, **205**, 114577.
29 S. H. Kim, H. C. Shum, J. W. Kim, J. C. Cho and D. A. Weitz, *J. Am. Chem. Soc.*, 2011, **133**, 15165–15171.
30 H. Zhang, J. Yang, R. Sun, S. Han, Z. Yang and L. Teng, *Acta Pharm. Sin. B*, 2023, **13**, 3277–3299.
31 N. Chen, S. Li, X. Li, Q. Zhan, L. Li, L. Long, J. Zhao, X. Hou and X. Yuan, *Chem. Eng. J.*, 2022, **429**, 132305.
32 H. Seo and H. Lee, *Nat. Commun.*, 2022, **13**, 5179.
33 X. Shi, M. Shen and H. Möhwald, *Prog. Polym. Sci.*, 2004, **29**, 987–1019.
34 C. Vranckx, L. Lambricht, V. Préat, O. Cornu, C. Dupont-Gillain and A. vander Straeten, *Langmuir*, 2022, **38**, 5579–5589.
35 J. Borges, J. Zeng, X. Q. Liu, H. Chang, C. Monge, C. Garot, K. Ren, P. Machillot, N. E. Vrana, P. Lavalle, T. Akagi, M. Matsusaki, J. Ji, M. Akashi, J. F. Mano, V. Gribova and C. Picart, *Adv. Healthcare Mater.*, 2024, **13**(8), 2302713.
36 Y. Huang, Y. Lin, X. Ran, J. Ren and X. Qu, *Nanoscale*, 2014, **6**, 11328–11335.
37 M. D. Klein and R. Langer, *Trends Biotechnol.*, 1986, **4**, 179–186.
38 Y. An, C. Ji, H. Zhang, Q. Jiang, M. F. Maitz, J. Pan, R. Luo and Y. Wang, *ACS Nano*, 2025, **19**, 11517–11546.
39 N. Jan, H. Shah and G. Shi, *Int. J. Pharm.*, 2025, **680**, 125753.
40 X. Du, J. Huang, C. Zhao, Z. Hu, L. Zhang, Z. Xu, X. Liu, X. Li, Z. Zhang, S. Guo, T. Yin and G. Wang, *Nanoscale*, 2025, **17**, 9738–9763.
41 Y. Chen, N. Douanne, T. Wu, I. Kaur, T. Tsering, A. Erzingatzian, A. Nadeau, D. Juncker, V. Nerguizian and J. V. Burnier, *Sci. Adv.*, 2025, **11**(9), eads5249.
42 H. Liu, Y. Li, Y. Wang, L. Zhang, X. Liang, C. Gao and Y. Yang, *Bioact. Mater.*, 2025, **47**, 481–501.
43 P. H. D. Nguyen, M. K. Jayasinghe, A. H. Le, B. Peng and M. T. N. Le, *ACS Nano*, 2023, **17**, 5187–5210.

44 P. M. Glassman, E. D. Hood, L. T. Ferguson, Z. Zhao, D. L. Siegel, S. Mitragotri, J. S. Brenner and V. R. Muzykantov, *Adv. Drug Delivery Rev.*, 2021, **178**, 113992.
45 H. Xiao, F. Raza, K. Li, J. Song, H. Zafar, S. Yang, J. Su and M. Qiu, *J. Controlled Release*, 2025, **383**, 113829.
46 N. Kostevšek, *Biomater. Adv.*, 2025, **170**, 214234.
47 P. N. Smith, L. Mao, K. Sinha and A. J. Russell, *Acta Biomater.*, 2021, **124**, 270–281.
48 Y. Chen, Y. Zhang, J. Zhuang, J. H. Lee, L. Wang, R. H. Fang, W. Gao and L. Zhang, *ACS Nano*, 2019, **13**, 7209–7215.
49 S. Zou, B. Wang, Q. Wang, G. Liu, J. Song, F. Zhang, J. Li, F. Wang, Q. He, Y. Zhu and L. Zhang, *ACS Appl. Mater. Interfaces*, 2022, **14**, 42454–42467.
50 S. Zou, Q. Wang, Q. He, G. Liu, J. Song, J. Li, F. Wang, Y. Huang, Y. Hu, D. Zhou, Y. Lv, Y. Zhu, B. Wang and L. Zhang, *J. Nanobiotechnol.*, 2023, **21**, 256.
51 K. Qin, F. Meng, D. Han, W. Guo, X. Li, Z. Li, L. Du, H. Zhou, H. Yan, Y. Peng and Z. Gao, *J. Nanobiotechnol.*, 2024, **22**, 593.
52 L. Poirier, L. Pinault, N. Armstrong, E. Ghigo, D. Daudé and E. Chabrière, *Chem. – Biol. Interact.*, 2019, **306**, 96–103.
53 B. Rémy, L. Plener, L. Poirier, M. Elias, D. Daudé and E. Chabrière, *Sci. Rep.*, 2016, **6**, 37780.
54 T. Pashirova, Z. Shaihutdinova, D. Tatarinov, M. Mansurova, R. Kazakova, A. Bogdanov, E. Chabrière, P. Jacquet, D. Daudé, A. A. Akhunzianov, R. R. Miftakhova and P. Masson, *Int. J. Mol. Sci.*, 2023, **24**, 15756.
55 T. Pashirova, Z. Shaihutdinova, D. Tatarinov, A. Titova, A. Malanyeva, O. Vasileva, K. Gabdurakhmanov, S. Dudnikov, L. M. Schopfer, O. Lockridge and P. Masson, *Int. J. Biol. Macromol.*, 2024, **282**, 137305.
56 S. Cerritelli, D. Velluto and J. A. Hubbell, *Biomacromolecules*, 2007, **8**, 1966–1972.
57 E. A. Scott, A. Stano, M. Gillard, A. C. Maio-Liu, M. A. Swartz and J. A. Hubbell, *Biomaterials*, 2012, **33**, 6211–6219.
58 D. Velluto, D. Demurtas and J. A. Hubbell, *Mol. Pharm.*, 2008, **5**, 632–642.
59 F. Worek, G. Reiter, P. Eyer and L. Szinicz, *Arch. Toxicol.*, 2002, **76**, 523–529.
60 T. N. Pashirova, A. S. Sapunova, S. S. Lukashenko, E. A. Burilova, A. P. Lubina, Z. M. Shaihutdinova, T. P. Gerasimova, V. I. Kovalenko, A. D. Voloshina, E. B. Souto and L. Y. Zakharova, *Int. J. Pharm.*, 2020, **575**, 118953.
61 A. Cornish-Bowden, *Fundamentals of Enzyme Kinetics*, Wiley-VCH, Weinheim, 4th edn, 2012.
62 J.-W. Yoo, D. J. Irvine, D. E. Discher and S. Mitragotri, *Nat. Rev. Drug Discovery*, 2011, **10**, 521–535.
63 G. M. Ihler, R. H. Glew and F. W. Schnure, *Proc. Natl. Acad. Sci. U. S. A.*, 1973, **70**, 2663–2666.
64 R. Hadi Barhaghtalab, H. Tanimowo Aiyelabegan, H. Maleki, F. Mirzavi, J. Gholizadeh Navashenaq, F. Abdi, F. Ghaffari and R. Vakili-Ghartavol, *Int. J. Pharm.*, 2024, **665**, 124658.
65 C. H. Villa, A. C. Anselmo, S. Mitragotri and V. Muzykantov, *Adv. Drug Delivery Rev.*, 2016, **106**, 88–103.
66 A. D. Peshkova, T. V. Brysgel, P. Mody, J. Nong, Z. Wang, J. W. Myerson, R. I. Litvinov, J. W. Weisel, J. S. Brenner, P. M. Glassman, O. A. Marcos-Contreras and V. R. Muzykantov, *Bioconjugate Chem.*, 2025, **36**, 263–275.
67 L. Pei, *Fundam. Appl. Toxicol.*, 1995, **28**, 209–214.
68 L. Pei, G. Omburo, W. D. Mcguinn, I. Petrikovics, K. Dave, F. M. Raushel, J. R. Wild, J. R. Deloach and J. L. Way, *Toxicol. Appl. Pharmacol.*, 1994, **124**, 296–301.
69 W. McGuinn, *Fundam. Appl. Toxicol.*, 1993, **21**, 38–43.
70 V. R. Muzykantov, *Expert Opin. Drug Delivery*, 2010, **7**, 403–427.
71 A. Choi, K. Javius-Jones, S. Hong and H. Park, *Int. J. Nanomed.*, 2023, **18**, 509–525.
72 C.-M. J. Hu, L. Zhang, S. Aryal, C. Cheung, R. H. Fang and L. Zhang, *Proc. Natl. Acad. Sci. U. S. A.*, 2011, **108**, 10980–10985.
73 B. T. Luk, C.-M. Jack Hu, R. H. Fang, D. Dehaini, C. Carpenter, W. Gao and L. Zhang, *Nanoscale*, 2013, **6**, 2730–2737.
74 Z. Wu, T. Li, J. Li, W. Gao, T. Xu, C. Christianson, W. Gao, M. Galarnyk, Q. He, L. Zhang and J. Wang, *ACS Nano*, 2014, **8**, 12041–12048.
75 T. Einfalt, M. Garni, D. Witzigmann, S. Sieber, N. Baltisberger, J. Huwyler, W. Meier and C. G. Palivan, *Adv. Sci.*, 2020, **7**(4), 1901923.
76 P. L. Luisi, T. P. de Souza and P. Stano, *J. Phys. Chem. B*, 2008, **112**, 14655–14664.
77 S. D. Varfolomeev, V. Švedas, E. N. Efremenko, A. M. Egorov, M. G. Khrenova, V. I. Tishkov, D. L. Atroshenko, A. A. Pometun, S. S. Savin, N. N. Ugarova, G. Y. Lomakina, I. V. Gachok, I. V. Lyagin, V. I. Muronetz, A. P. Sinitsyn, O. A. Sinitsyna, A. M. Rojhkova, G. F. Makhaeva, S. O. Bachurin, O. I. Lavrik, D. O. Zharkov, A. V. Yudkina, O. M. Panasenko, A. A. Baykov, P. Masson, T. N. Pashirova, Z. M. Shaihutdinova, E. V. Popova, V. E. Tikhomirova, O. A. Kost, E. V. Kudryashova, N. V. Dobryakova, N. L. Klyachko, M. M. Veselov, A. V. Lopukhov, I. M. Le-Deygen, A. D. Usvaliev, I. V. Chudosai, N. L. Eremeev, M. E. Zvereva, M. Y. Rubtsova, M. M. Ulyashova, G. V. Presnova, L. V. Sigolaeva, D. V. Pergushov, I. N. Kurochkin, E. G. Evtushenko, I. A. Boginskaya, Y. Y. Zvyagina, E. A. Slipchenko, O. V. Kryukova, M. V. Sedova, I. A. Ryzhikov, V. V. Shumyantseva, P. I. Koroleva, T. V. Bulko, L. E. Agafonova, R. A. Masamrekh, T. A. Filippova, A. V. Kuzikov, A. P. Savitsky, M. O. Shleeva, I. D. Solovyev and N. K. Marynich, *Russ. Chem. Rev.*, 2024, **93**, RCR5144.
78 H. M. Piwonski, M. Goomanovsky, D. Bensimon, A. Horovitz and G. Haran, *Proc. Natl. Acad. Sci. U. S. A.*, 2012, **109**(22), E1437–E1443.
79 T. N. Pashirova, D. A. Tatarinov, M. V. Gabova, S. N. Batasheva, V. N. Kuryakov, Z. M. Shaihutdinova, V. F. Mironov and P. Masson, *Colloid J.*, 2025, **87**(6), accepted.
80 T. Sunami, K. Hosoda, H. Suzuki, T. Matsuura and T. Yomo, *Langmuir*, 2010, **26**, 8544–8551.
81 T. Sunami, N. Ichihashi, T. Nishikawa, Y. Kazuta and T. Yomo, *ChemBioChem*, 2016, **17**, 1282–1289.
82 P. L. Luisi, M. Allegretti, T. Pereira de Souza, F. Steiniger, A. Fahr and P. Stano, *ChemBioChem*, 2010, **11**, 1989–1992.
83 T. P. de Souza, A. Fahr, P. L. Luisi and P. Stano, *J. Mol. Evol.*, 2014, **79**, 179–192.

84 P. Walde and B. Marzetta, *Biotechnol. Bioeng.*, 1998, **57**, 216–219.
85 M. Li, M. J. Hanford, J.-W. Kim and T. L. Peeples, *J. Biol. Eng.*, 2007, **1**, 4.
86 M. A. Luna, J. J. Silber, L. Sereno, N. M. Correa and F. Moyano, *RSC Adv.*, 2016, **6**, 62594–62601.
87 A. C. Anselmo, V. Gupta, B. J. Zern, D. Pan, M. Zakrewsky, V. Muzykantov and S. Mitragotri, *ACS Nano*, 2013, **7**, 11129–11137.
88 J. S. Brenner, D. C. Pan, J. W. Myerson, O. A. Marcos-Contreras, C. H. Villa, P. Patel, H. Hekierski, S. Chatterjee, J.-Q. Tao, H. Parhiz, K. Bhamidipati, T. G. Uhler, E. D. Hood, R. Y. Kiseleva, V. S. Shuvaev, T. Shuvaeva, M. Khoshnejad, I. Johnston, J. V. Gregory, J. Lahann, T. Wang, E. Cantu, W. M. Armstead, S. Mitragotri and V. Muzykantov, *Nat. Commun.*, 2018, **9**, 2684.
89 E. Chambers and S. Mitragotri, *Exp. Biol. Med.*, 2007, **232**, 958–966.
90 D. C. Pan, J. W. Myerson, J. S. Brenner, P. N. Patel, A. C. Anselmo, S. Mitragotri and V. Muzykantov, *Sci. Rep.*, 2018, **8**, 1615.
91 G. Bosman, F. Willekens and J. Werre, *Cell. Physiol. Biochem.*, 2005, **16**, 1–8.
92 Q.-V. Le, J. Lee, H. Lee, G. Shim and Y.-K. Oh, *Acta Pharm. Sin. B*, 2021, **11**, 2096–2113.
93 B. Jia, Y. Shi, Y. Yan, H. Shi, J. Zheng and J. Liu, *Adv. Biol.*, 2025, **9**(5), e2400242.